Wood Sci Technol (2008) 42:633–647
DOI 10.1007/s00226-008-0192-7

ORIGINAL

Three-dimensional elastic behaviour of common yew and Norway spruce

Daniel Keunecke · Stefan Hering · Peter Niemz

Received: 6 August 2007 / Published online: 26 April 2008

Abstract In view of its high density, yew wood has a remarkably low longitudinal Young's modulus, which makes it unique among coniferous woods. However, the elastic response of yew related to other load directions is largely unknown. Therefore, our goal was to comprehensively characterise the three-dimensional elastic behaviour of yew wood. To achieve this, we performed tensile tests on dog-bone-shaped yew specimens and determined the three Young's moduli and six Poisson's ratios using a universal testing machine and a digital image correlation technique. All tests were also applied to spruce as reference species. After including the shear moduli determined in a prior study by our group, all elastic engineering parameters of yew and spruce were ascertained. Based on these values, the three-dimensional elastic behaviour was describable with deformation bodies and polar diagrams. Evaluating these illustrations revealed that yew had a lower stiffness only in the longitudinal direction. In all other three-dimensional directions, spruce was clearly more compliant than yew. Particularly, in the radial–tangential plane, both species varied largely in their degree of anisotropic elasticity. All mentioned differences between yew and spruce originate at the microstructural level.

Introduction

Yew wood was a very popular longbow wood for hundreds of years, since it fulfils particularly one condition: it is flexible. In the load case of a longbow, 'flexibility' means, in technical terms, a low longitudinal Young's modulus (E_L) with simultaneously large strains in the elastic range. Several literary sources document the relatively low axial stiffness of yew (6,200–12,000 MPa) determined in static

D. Keunecke (✉) · S. Hering · P. Niemz
Institute for Building Materials (Wood Physics Group), ETH Zurich,
Schafmattstrasse 6, 8093 Zurich, Switzerland
e-mail: danielk@ethz.ch

tests (e.g., Sekhar and Sharma 1959; Jakubczyk 1966; Wagenführ 2000; Keunecke et al. 2007a). In view of its high raw density (620–720 kg m^{-3} at 11–12% equilibrium moisture content), this compliant behaviour makes yew wood unique among gymnosperms and an interesting case study for further comprehensive research into its elasticity.

However, clearly less is known about the elastic response of yew related to other load directions. In a first approach, we determined the Young's and shear moduli of yew and spruce by means of ultrasonic waves (Keunecke et al. 2007b). The radial (E_R) and tangential (E_T) Young's moduli were 2.0–2.3 times higher for yew than for spruce due to the high density, which was even more intensely reflected in the shear moduli: G_{LR} and G_{LT} were three times and G_{RT} six times higher for yew. Since our concern is the complete elasto-mechanical characterisation of yew wood, two aspects have to be considered:

- It is well known that the Young's moduli determined dynamically are overestimated in contrast to the shear moduli, which are in the same range as the statically determined values.
- The stress–strain relations of wood, regarded as a rhombic crystalline system, are based on 12 compliance coefficients s_{ij}. For their calculation, a full set of so-called elastic engineering parameters (also referred to as elastic constants) must be available. Thus, in addition to the Young's and shear moduli, the Poisson's ratios ν_{ij} are also required.

In the present study, therefore, we designed an appropriate "dog-bone" specimen shape and determined the three Young's moduli and six Poisson's ratios of yew (*Taxus baccata* L.) in uniaxial tensile tests at standard climatic conditions (20°C, 65% RH). By this means and by taking into account the shear moduli in our prior study, further interpretation of the three-dimensional elastic behaviour was possible, even when the load axis did not coincide with one of the three orthotropic axes L, R and T. For wood, the principle of the latter was shown for the first time by Hörig (1933) and illustrated in polar diagrams. So as to serve as a reference species and as a basis for discussion, all of our investigations and evaluations have also been applied to Norway spruce (*Picea abies* [L.] Karst.). Its mechanical properties are well documented in numerous studies, which proved helpful towards appraising the validity of our results.

In the wood sector, the first sets of elastic engineering parameters have been determined for spruce (Carrington 1923; Schlüter 1932; Krabbe 1960; Neuhaus 1981). In the meantime, full sets of further softwoods and hardwoods, partly tropical species, are available. While the determination of Young's moduli is relatively uncomplicated (e.g., in tensile tests), the shear moduli require much more effort. Direct determination with cubes or discs and indirect determination by means of torsion are reported, as well as the dynamic procedures such as ultrasound and eigenfrequency.

Because of the difficulty in measuring small strains precisely, the Poisson's ratios of relatively few wood species are available from literature. They have typically been determined using strain gages or inductive strain measurements so far. In this study, a non-contacting optical surface deformation measurement method was

chosen. The major advantages of this digital image correlation (DIC) technique are as follows: (1) the measurement process does not influence the behaviour of the specimen during the test; (2) no restrictions exist regarding the specimen size and geometry; (3) full-field measurements cover inhomogeneous surface deformations as is likely to be present in wood.

With this study, we wanted to

- describe the three-dimensional elastic behaviour of yew wood
- evaluate the main differences between yew and spruce regarding their elasticity
- verify if the chosen experimental setup is appropriate to determine the Young's moduli and Poisson's ratios of wood

Material and methods

Raw material

The centrepieces of the specimens (Fig. 1a) were cut from five yew and five spruce stems (at breast height) grown at stands close to Zurich, Switzerland. The samples were taken from the outer heartwood region where the anatomical structure is approximately orthotropic. Samples containing compression wood were omitted. The 45 centrepieces per species were oriented as follows: 15 × longitudinal (L), 15 × radial (R), 15 × tangential (T).

Specimen composition and shape

Only boards with a thickness of 60–70 mm were available for specimen production; thus, the length in the R and T directions was limited. Since we wanted to produce

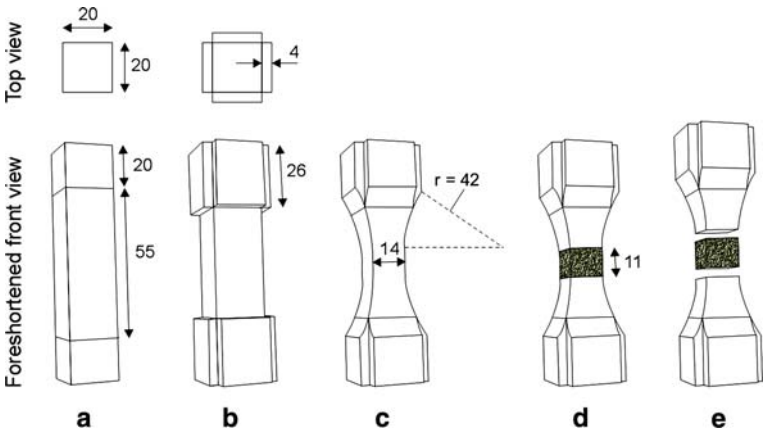

Fig. 1 Specimen preparation: **a** extending the top and bottom ends of the centrepieces by cubes; **b** reinforcing the ends by beech plates; **c** generating a dog-bone shape using a router; **d** applying a speckle-pattern; **e** separating the central part for density measurement. All dimensions in mm

dog-bone-shaped specimens, as they are preferably used in tensile tests, the specimens had to be scaled up to ensure that a feasible minimum number of growth rings were present in the narrow section of the specimens. An influence of inhomogeneity caused by earlywood (EW) and latewood (LW) zones could be reduced this way. Therefore, the centrepieces were extended by gluing cubes of 20 mm edge length to their ends (Fig. 1a). A two-component epoxy adhesive (Araldite) was used for this purpose. The cubes were of the same wood species as the centrepieces and oriented in the same principle directions. Small beech plates were glued onto the specimens' ends as lateral reinforcement and to enlarge the load transmission area using again the Araldite adhesive (Fig. 1b). The four-sided dog-bone specimen shape (Fig. 1c) was achieved by a contour template and a router. Consequently, the specimens had vertical and horizontal axes of symmetry. The cross-sectional area in the narrow specimen section was 14 mm × 14 mm. The section of planar, parallel running specimen surfaces was 11 mm long in the load direction.

Speckle pattern

In the narrow planar specimen section, a filmy high-contrast random dot texture (a "speckle pattern") of 11 mm × 14 mm was sprayed on two adjacent sides of the specimen (Fig. 1d). To obtain very fine speckles and therefore a high-resolution pattern, an airbrush gun and finely pigmented acrylic paint was used. First, a white ground coat and then black speckles were applied, resulting in a speckle pattern of heterogeneous grey values. This pattern was needed for the evaluation of displacements on the specimen's surface during tensile testing by means of the DIC software.

Tensile testing

After the specimens had reached an equilibrium moisture content at 20°C and 65% RH, tensile tests were performed using a Zwick Z100 (Schenck) universal testing machine. A load cell with 100 kN maximum capacity was used for L specimens and a 1 kN load cell for R and T specimens. Data acquisition began when a defined pre-load was reached. The tensile tests were performed only at small strains in the linear elastic range. To ensure that plastic deformation was avoided, the specimens were unloaded again at 15% of the predicted maximum load, which had been estimated in preliminary tests. The feed rate was defined such that the maximum load would theoretically be reached in 90 (± 30) s. A total of four loading–unloading cycles was applied to each specimen.

Strain measurement

During tensile testing, one of both speckle fields was filmed by a CCD camera with a distortion-free objective. Vibrations of the camera were avoided. The principle axis of the camera was accurately aligned perpendicular to the specimen surface. The speckle field (11 mm × 14 mm, Fig. 1e) was resolved with about

650 × 830 pixels. The image sequences were recorded with a frequency of 4–8 s^{-1} and saved as TIF files. A cold light source provided even illumination of the speckle field, thereby, too strong reflections from the specimen surface were avoided, which is required for the exact tracking of surface deformation.

After two loading–unloading cycles, the second speckle field was filmed. Exemplified by an L specimen, this means that the camera films the deformations twice on the LR surface and twice on the LT surface.

For subsequent evaluations, the data from the four TIF series per specimen were run through a strain mapping software (VIC 2D, Correlated Solutions) that computed the two-dimensional strain from the surface deformations. The displacements are calculated on the basis of a cross-correlation algorithm. Using the grey value pattern in a defined neighbourhood (the "subset") around a central pixel, the algorithm locates the best matching pattern after deformation by maximising the cross-correlation between two subsets. By means of the displacement gradients, strains can be accurately resolved. The resolution of displacement is of the order of 1/100th of a pixel.

After computing the two-dimensional strain, the average strain in the load direction and the average contraction transverse to the load direction was calculated.

Calculation of Young's moduli

The Young's modulus E is the ratio of stress (σ) to corresponding strain (ε) when the material behaves elastically (Eq. 1). It is represented by the slope of the initial straight segment of the stress–strain diagram:

$$E = \Delta\sigma/\Delta\varepsilon. \tag{1}$$

The average stress–strain curve of four loading–unloading cycles in the elastic range was calculated for each specimen.

Calculation of Poisson's ratios

The phenomenon that lateral contraction of a rod occurs as it elongates is called Poisson's effect. The ratio of passive (=contraction) to active (=elongation) strain is defined as Poisson's ratio v_{ij}:

$$v_{ij} = -\varepsilon_i/\varepsilon_j, \tag{2}$$

where i refers to the direction of lateral contraction and j to load-directional elongation. Transverse contraction was plotted against load directional strain. The slope of the linear regression multiplied by (-1) corresponds to the Poisson's ratio. This time, the mean value is based on two measurements.

Calculation of compliance coefficients

Derived from Voigt's (1928) disquisition on crystal physics, Hörig (1933) idealised wood as rhombic crystalline material with distinctively different directional

properties related to three orthotropic axes (L, R, T). In such an anisotropic system, 12 compliance coefficients s_{ij} are required to describe the three-dimensional elastic behaviour when the geometric and orthotropic axes coincide. A common notation of Hooke's law is the compliance matrix equation where strains are stated as linear functions of stresses:

$$\begin{pmatrix} \varepsilon_1 \\ \varepsilon_2 \\ \varepsilon_3 \\ \gamma_{23} \\ \gamma_{13} \\ \gamma_{12} \end{pmatrix} = \begin{bmatrix} s_{11} & s_{12} & s_{13} & 0 & 0 & 0 \\ s_{21} & s_{22} & s_{23} & 0 & 0 & 0 \\ s_{31} & s_{32} & s_{33} & 0 & 0 & 0 \\ 0 & 0 & 0 & s_{44} & 0 & 0 \\ 0 & 0 & 0 & 0 & s_{55} & 0 \\ 0 & 0 & 0 & 0 & 0 & s_{66} \end{bmatrix} \begin{pmatrix} \sigma_1 \\ \sigma_2 \\ \sigma_3 \\ \tau_{23} \\ \tau_{13} \\ \tau_{12} \end{pmatrix}. \tag{3}$$

By using the concept of strain energy, the 12 compliance coefficients can be even further simplified to nine independent coefficients ($s_{12} = s_{21}$, $s_{13} = s_{31}$, $s_{23} = s_{32}$). For details, see for example Bodig and Jayne (1993). The diagonal coefficients s_{ij} ($i = j$) are reciprocals of the Young's and shear moduli (the notation is adapted according to Hörig (1933)):

$$s_{11} = E_{\mathrm{T}}^{-1},\ s_{22} = E_{\mathrm{L}}^{-1},\ s_{33} = E_{\mathrm{R}}^{-1},\ s_{44} = G_{\mathrm{LR}}^{-1},\ s_{55} = G_{\mathrm{TR}}^{-1},\ s_{66} = G_{\mathrm{TL}}^{-1}. \tag{4}$$

The non-diagonal coefficients s_{ij} ($i \neq j$) are defined as follows:

$$\begin{aligned} &s_{21} = s_{11} \cdot -\nu_{\mathrm{LT}},\ s_{31} = s_{11} \cdot -\nu_{\mathrm{RT}},\ s_{12} = s_{22} \cdot -\nu_{\mathrm{LT}},\ s_{32} = s_{22} \cdot -\nu_{\mathrm{RL}}, \\ &s_{13} = s_{33} \cdot -\nu_{\mathrm{TR}},\ s_{23} = s_{33} \cdot -\nu_{\mathrm{LR}}. \end{aligned} \tag{5}$$

Consequently, all compliance coefficients can also be expressed in terms of engineering elastic parameters:

$$\begin{pmatrix} \varepsilon_T \\ \varepsilon_L \\ \varepsilon_R \\ \gamma_{LR} \\ \gamma_{TR} \\ \gamma_{TL} \end{pmatrix} = \begin{bmatrix} \frac{1}{E_T} & -\frac{\nu_{LT}}{E_L} & -\frac{\nu_{RT}}{E_R} & 0 & 0 & 0 \\ -\frac{\nu_{TL}}{E_T} & \frac{1}{E_L} & -\frac{\nu_{RL}}{E_R} & 0 & 0 & 0 \\ -\frac{\nu_{TR}}{E_T} & -\frac{\nu_{LR}}{E_L} & \frac{1}{E_R} & 0 & 0 & 0 \\ 0 & 0 & 0 & \frac{1}{G_{LR}} & 0 & 0 \\ 0 & 0 & 0 & 0 & \frac{1}{G_{TR}} & 0 \\ 0 & 0 & 0 & 0 & 0 & \frac{1}{G_{TL}} \end{bmatrix} \begin{pmatrix} \sigma_T \\ \sigma_L \\ \sigma_R \\ \tau_{LR} \\ \tau_{TR} \\ \tau_{TL} \end{pmatrix}. \tag{6}$$

Density and moisture content

The central cuboid was cut out of each specimen (Fig. 1e) and used for gravimetrical density determination. In this manner, the density of the load-carrying narrow section of the specimens was measured. For the calculation of the moisture content ω (Eq. 7), the mass of the cuboids was determined at 20°C/65% RH (m_ω) and oven-dry (m_0):

$$\omega = (m_\omega - m_0) \cdot m_0^{-1}. \tag{7}$$

Results and discussion

Strain measurement

In a preceding evaluation step, the deformation of various sub-areas reduced to one-third of the full speckle field was analysed exemplarily. It was found that – independent from the sub-area position – the strains of sub-areas and the full speckle field were almost identical. Furthermore, there was (if at all) minimal difference between the four individual stress–strain curves measured per specimen.

A representative example for the strain data of a full loading–unloading cycle provided by the DIC software is shown in Fig. 2. In this case, a yew specimen was loaded longitudinally and the deformations on the LR surface were analysed, i.e., the mean longitudinal strain and mean radial contraction were computed. Even the development of small strains (in this example up to 0.12% and −0.06%) was reliably trackable due to the sub-pixel accurate algorithm. In Fig. 3, longitudinal strain is plotted against radial contraction for the same data set as shown in Fig. 2. The values decrease in an acceptable narrow path. The slope of the linear regression (in this case −0.46) multiplied by (−1) corresponds to the Poisson's ratio ν_{RL}.

The aforementioned observations indicate that the specimen shape and the experimental boundary conditions were appropriate for our purposes. Nevertheless, using a second CCD camera and averaging simultaneous strain measurements on the front and back side of the specimen certainly would increase the accuracy of the results.

Young's moduli

Table 1 provides an overview of the determined elastic engineering parameters. Even though 15 specimens per species and orientation were prepared, the number

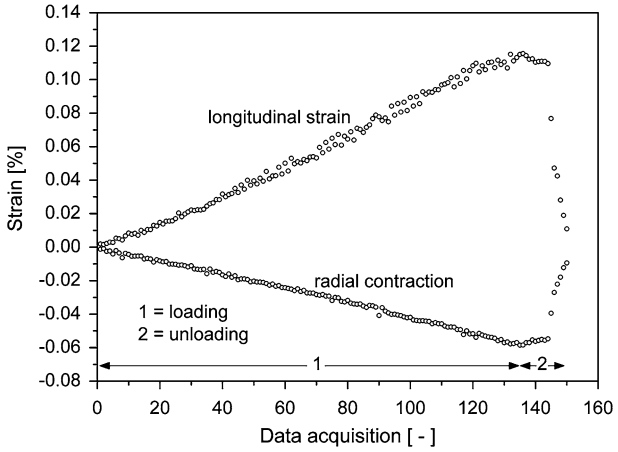

Fig. 2 Mean longitudinal strain and mean radial contraction of a loading–unloading cycle computed for a longitudinal specimen

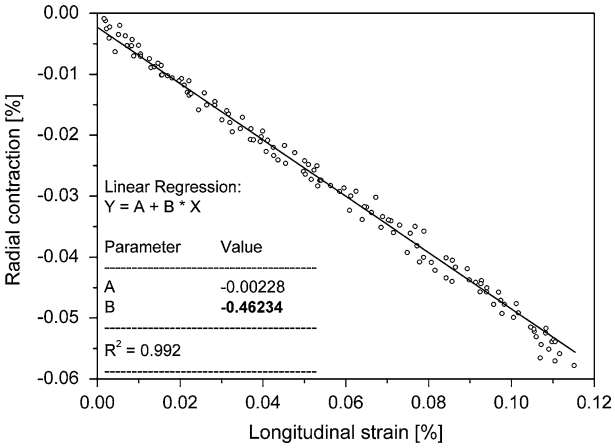

Fig. 3 Radial contraction versus longitudinal strain for the same data set as shown in Fig. 2

eventually used for data interpretation is partly reduced. In a few cases, the adhesive was not completely hardened, probably due to a slightly deviant mixture ratio between resin and hardener.

The Young's moduli of spruce are roughly in the range of literature references (Table 2). The mean E_L was lower for yew than for spruce (10,500 vs. 12,800 MPa). Calculating the specific E_L (=E_L related to raw density) would reveal an even larger difference between both species (17,000 vs. 27,200 MPa/kg m^{-3}). This is in agreement with our previous studies where we measured E_L of both species in three-point bending (Keunecke et al. 2007a) and dynamically (Keunecke et al. 2007b). Our current investigations with different techniques (X-ray scattering, pit aperture method) suggest that the microfibril angle (MFA) of the S_2 tracheid layer is clearly larger in yew (particularly in LW tracheids) and therefore causes, despite the high density, the low axial stiffness. This relationship between MFA and stiffness is well known and has been shown, for example, by Reiterer et al. (1999).

In contrast, E_R and E_T were about 50% higher for yew compared to spruce. By means of ultrasonic waves, a 100–130% higher transverse stiffness was determined for yew than for spruce (Keunecke et al. 2007b). Wedge splitting tests performed on both species (Keunecke et al. 2007c) even revealed a 300% higher stiffness for yew. In that special case, however, this was influenced by the specimen geometry and the presence and position of a starter notch. As becomes clear, transverse stiffness can vary strongly due to the natural heterogeneity of the wood and depending on the measurement method. Nevertheless, in all cases, it was clearly higher for yew than for spruce, predominantly as a result of the high density. Current evaluation of high-resolution X-ray density profiles reveals that particularly the EW zones of yew are clearly denser (500–600 kg m^{-3}) than those of spruce (250–300 kg m^{-3}) while the LW density is similar for both species (900–1,000 kg m^{-3}) (Fig. 4). However, to a certain extent, the higher transverse stiffness of yew can also be explained by its higher MFA. Considering the drastic differences between G_{RT} of yew and spruce, it

Table 1 Elastic engineering parameters determined in uniaxial tension

	Number of specimens n	Density ρ (g cm^{-3})	Young's modulus E (MPa)	Poisson's ratios (–)			
				ν_{RL}	ν_{TL}	ν_{TR}	ν_{RT}
Yew							
L							
$\bar{x}$	12	0.62	10,500	0.46	0.48	–	–
CoV (%)		5.7	13.6	13.2	25.9		
R							
$\bar{x}$	15	0.63	927	–	–	0.50	–
CoV (%)		6.3	24.6			14.8	
T							
$\bar{x}$	14	0.62	627	–	–	–	0.20
CoV (%)		6.1	17.5				30.6
Spruce							
L							
$\bar{x}$	10	0.47	12,800	0.36	0.45	–	–
CoV (%)		7.2	9.2	13.2	8.2		
R							
$\bar{x}$	13	0.48	625	–	–	0.48	–
CoV (%)		6.6	20.4			19.2	
T							
$\bar{x}$	11	0.46	397	–	–	–	0.21
CoV (%)		7.2	10.3				16.8

$\bar{x}$ mean value, *CoV* coefficient of variation

seems likely that the species differ in further submicroscopic parameters such as matrix composition or cell/cell adhesion.

The lower axial and higher transverse stiffness of yew is of course reflected in the quotients E_L/E_R (=11 for yew and =21 for spruce) and E_L/E_T (=17 for yew and =32 for spruce), which emphasise the large discrepancy between both species. A further anatomical feature causes a ratio E_R/E_T of 1.5 for yew and 1.6 for spruce: wood rays reinforce the tissue in the radial direction (Burgert 2000).

Poisson's ratios

According to Bodig and Jayne (1993), Poisson's ratios do not seem to vary with density or other anatomical characteristics of wood in any recognisable fashion. This may explain why we did not find considerable differences between both species in this respect (Table 1). Only ν_{RL} was higher for yew (0.46) than for spruce (0.36). In view of the small number of specimens, not too much should be read into this difference. ν_{RL}, ν_{TL} and ν_{TR} of spruce are comparable with literature references (Table 2). ν_{RT}, however, was smaller (0.20 for yew and 0.21 for spruce), resulting in a ratio ν_{TR}/ν_{RT} of 2.3 for spruce and 2.5 for yew. According to Eq. 8

Table 2 Elastic engineering and compliance parameters: comparison of our mean values and literature references

	Moisture content ω (%)	Compliance parameters				Elastic engineering parameters				Anisotropy(E_L/E_T)/(E_L/E_R)/(E_R/E_T) (–)
		$s_{11}/s_{22}/s_{33}$ (Pa^{-1})	$s_{44}/s_{55}/s_{66}$ (Pa^{-1})	$-s_{23}/-s_{13}/-s_{12}$ (Pa^{-1})	$-s_{32}/-s_{31}/-s_{21}$ (Pa^{-1})	$E_T/E_L/E_R$ (MPa)	$G_{LR}/G_{RT}/G_{LT}$ (MPa)	$\nu_{LR}/\nu_{TR}/\nu_{TL}$ (–)	$\nu_{RL}/\nu_{RT}/\nu_{LT}$ (–)	
Our measurements										
Yew	11	1,590/95/1,080	575/2,720/606	44/535/46	44/324/46	627/10,500/927	1,740/368/1,650	0.041/0.50/0.48	0.46/0.20/0.029	17/11/1.5
Spruce	12	2,520/78/1,600	1,621/18,900/1,700	28/768/35	28/528/35	397/12,800/625	617/53/587	0.018/0.48/0.45	0.36/0.21/0.014	32/21/1.6
Literature references										
Spruce (Hörig 1933)	10	2,500/62/1,430	1,590/27,000/1,290	27/600/33	27/600/33	400/16,200/699	628/37/775	0.019/0.42/0.54	0.44/0.24/0.013	41/23/1.7
Spruce (Krabbe 1960)	12	2,330/88/902	1,350/27,500/1,460			430/11,400/1,110	742/36/686			27/10/2.6
Spruce (Neuhaus 1981)	12	2,380/83/1,220	1,600/23,600/1,350	68/732/46	37/740/84	420/12,000/818	623/42/743	0.056/0.60/0.55	0.41/0.31/0.035	29/15/1.9
Spruce (Wommelsdorff 1966)	14	2,330/89/1,020		50/598/50	40/606/65	429/11,300/980		0.049/0.59/0.56	0.45/0.26/0.028	26/12/2.3
Softwoods (Bodig and Jayne 1993)								0.041/0.47/0.42	0.37/0.35/0.033	

The shear moduli in the first (yew) and second row (spruce) have been determined my means of ultrasonic waves in a prior study (Keunecke et al. 2007b)

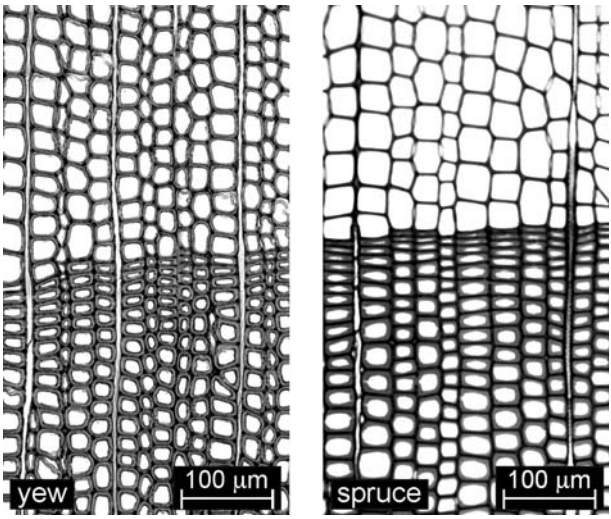

Fig. 4 Distinct density differences between EW zones of yew and spruce

$$\nu_{TR} \cdot \nu_{RT}^{-1} = E_R \cdot E_T^{-1}, \tag{8}$$

ν_{TR}/ν_{RT} should theoretically be approximately 1.5 taking the determined Young's moduli into account. This deviation due to the small ν_{RT} probably results from the specimen geometry. Especially for tangential specimens, it is difficult to ensure that the growth rings are arranged absolutely parallel to the load direction over the whole specimen length. A solution to this problem could be to produce specimens from several laminated layers to optimise the orthotropic orientation [as done by Krabbe (1960) or Neuhaus (1981)]. In this study, it was our intention to forgo lamellation to avoid an influence by the adhesive on the elastic behaviour.

Since the contraction was too small for a satisfactory resolution with the DIC software, ν_{LR} and ν_{LT} were not gaugeable. This is a well known problem in the field of materials testing (Bodig and Jayne 1993). Therefore, it is a common practise to calculate ν_{LR} and ν_{LT} according to the following relationship:

$$\nu_{LR} = \nu_{RL} \cdot E_R \cdot E_L^{-1} \quad \text{and} \quad \nu_{LT} = \nu_{TL} \cdot E_T \cdot E_L^{-1}. \tag{9}$$

$\nu_{LR} = 0.041$ and $\nu_{LT} = 0.029$ for yew, as well as $\nu_{LR} = 0.018$ and $\nu_{LT} = 0.014$ for spruce are obtained from Eq. 9.

Compliance parameters s_{ij}

Table 2 provides an overview of the determined elastic engineering and compliance parameters. The shear moduli are added from our previous study (Keunecke et al. 2007b), where specimens from the same stems as used in this study were tested. Furthermore, literature references for spruce and softwoods in general are listed in the table. One should note that $-s_{21}$ and $-s_{23}$ were calculated according to Eq. 5, i.e., by means of the calculated Poisson's ratios ν_{LT} and ν_{LR}. Consequently, the

numerical values of $-s_{12}$ and $-s_{21}$ are identical, as are the numerical values for $-s_{23}$ and $-s_{32}$. The asymmetry between $-s_{13}$ and $-s_{31}$ results again from the ratio ν_{TR}/ν_{RT}. The mean value ($-s_{13} = -s_{31} = 430$ Pa^{-1} for yew and 648 Pa^{-1} for spruce) would probably be closer to the actual value. Alternatively, ν_{RT} may be adjusted to two-thirds the value of ν_{TR}.

Three-dimensional elastic behaviour

The compliance matrix (Eq. 3) is only valid when stresses and strains are related to the principle growth directions L, R and T. If they deviate from these axes, the equations describing stress and strain have to be transformed to obtain a statement of Hooke's law in a three-dimensional coordinate system. A detailed description of the transformation procedure and a first-time spatial illustration as 'deformation bodies' can be found in Grimsel (1999). Two-dimensional sections through these bodies (as polar diagrams of the LR, LT and RT planes) were already derived at an early stage by Hörig (1933) on the basis of Voigt's (1928) textbook on crystal physics.

In Fig. 5, such deformation bodies are presented for yew and spruce based on coordinate transformations using our values s_{ij} in Table 2. They have to be interpreted as follows: To any arbitrary chosen axis in the three-dimensional coordinate system representing the L, R and T directions of a wood species, an identical tensile load is applied. The bodies illustrate the degree of deformation depending on the load direction.

A conspicuous anisotropy of spruce is obvious, as also shown by Grimsel (1999). The anisotropy of yew is clearly less pronounced; the deformation body rather resembles those shown by Grimsel for beech or mahogany. This is remarkable since, according to Grimsel, all deformation bodies evaluated so far for softwoods show similar characteristics and can clearly be distinguished from those of deciduous trees.

According to Bodig and Jayne (1993), however, comparison of experiment and theory has shown that a three-dimensional transformation is not always reliable for

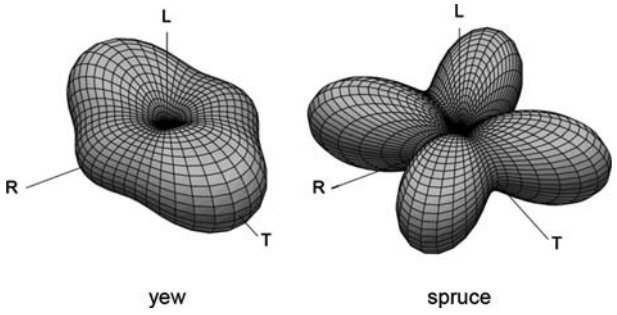

Fig. 5 Deformation bodies for yew and spruce. The scale of the axes is adjusted to the respective maximum deformation and thus not identical for both diagrams. Using the same scale would increase the spruce body to the 2.5-fold size (see also Fig. 6)

wood, while transformations in the principle planes are usually quite satisfactory. Nevertheless, in our opinion, deformation bodies are a valuable visual aid. Using appropriate software allows their rotation; examination of different perspectives assists in visualising and estimating the approximate spatial elastic characteristics of a wood species.

Two-dimensional polar diagrams (Fig. 6) show that yew and spruce only slightly diverge in the LR and LT plane. The general run of the curves is quite similar even though at a different scale. In contrast, the curves completely differ in the RT plane. Here, the deformation of spruce is highly anisotropic: Even small deviations from the principle axes cause a considerable increase of compliance at the same stress level. The maximum value (a multiple of the deformation along the R and T axes) is reached at an angle of about 45° as a result of the small G_{RT}. Yew behaves completely different: the deformation is largest on the T and R axes and slightly decreases to a minimum near 45°. Several factors may contribute to the lower directional dependence:

- The density variations between EW and LW are small compared to spruce (Fig. 4).
- The ratios G_{RT}/E_R and G_{RT}/E_T are clearly higher for yew than for spruce.

Moreover, the tracheids of yew are up to one-third smaller in length and diameter and also show a slightly more rounded cell shape (even in zones free of compression wood) compared to spruce. These aspects possibly support the more homogeneous deformation in the RT plane as well.

Both types of diagrams reveal that the only load direction, where yew is more compliant than spruce, is the L direction and a narrow range around it. However, this just accounts for a fraction of the whole three-dimensional body. In the

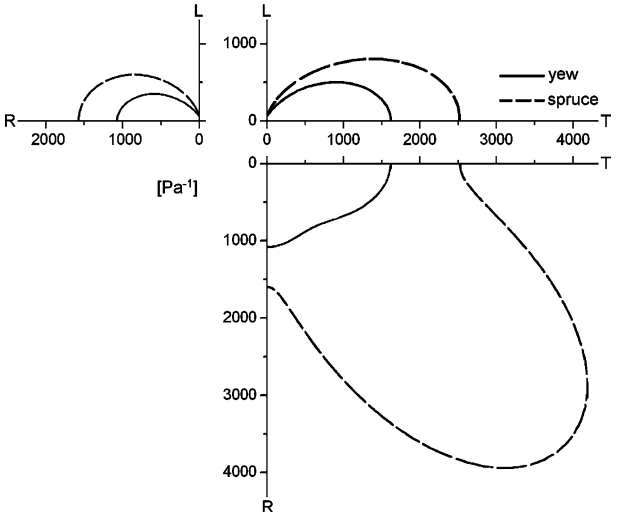

Fig. 6 Load-directional dependence of compliance in the principle planes illustrated in three polar diagrams. Each diagram represents a quarter circle

remaining directions yew is clearly stiffer than spruce. This again indicates the enormous impact of the MFA on longitudinal stiffness.

Conclusion

Our results confirm the lower axial and higher transverse stiffness of yew compared to spruce. This present and a prior study by our group complement each other and provide insight into the three-dimensional elasticity of both species. Illustrations such as the three-dimensional deformation bodies assisted in obtaining a general idea of their characteristic spatial compliance. Polar diagrams of the three principle orthotropic planes revealed that the main differences between both species regarding anisotropy are located in the RT plane. Based on both illustration options, yew wood turned out to behave clearly less anisotropic compared to spruce (and probably also compared to most other gymnosperms). Only in the longitudinal direction did yew have a lower stiffness. In all other three-dimensional directions, spruce was clearly more compliant than yew.

The chosen experimental setup was basically well suited to determine the Young's moduli and Poisson's ratios of yew and spruce at small strains, even though it leaves room for further development. The specimen shape was appropriate; solely in the case of tangential specimens should improvement measures such as lamellation be considered. With regard to statistical significance, however, a larger number of specimens would be desirable, but this was limited as a consequence of the time-consuming preparation. The accuracy of strain measurement based on the combination speckle pattern/CCD camera/DIC software turned out satisfactory for our purposes with a reasonably short computing time.

The main focus of our future investigations will be directed at the question: Is the low axial stiffness of yew also present at lower hierarchical levels (such as microtome sections or individual tracheids)?

Acknowledgments This work was supported by the European Cooperation in the field of Scientific and Technical Research (COST, Action E35).

References

Bodig J, Jayne BA (1993) Mechanics of wood and wood composites. Krieger Publishing Company, Malabar, p 712

Burgert I (2000) Die mechanische Bedeutung der Holzstrahlen im lebenden Baum. Dissertation, Hamburg, p 173

Carrington H (1923) The elastic constants of spruce. Philos Mag 45:1055–1057

Grimsel M (1999) Mechanisches Verhalten von Holz: Struktur- und Parameteridentifikation eines anisotropen Werkstoffes. Dissertation, Dresden, p 89

Hörig H (1933) Zur Elastizität des Fichtenholzes. 1. Folgerungen aus Messungen von H. Carrington an Spruce. Z Tech Phys 12:369–379

Jakubczyk B (1966) Technical properties of the yew wood from the preserve Wierzchlas. Sylwan 10:79–86

Keunecke D, Märki C, Niemz P (2007a) Structural and mechanical properties of yew wood. Wood Res 52:23–38

Keunecke D, Sonderegger W, Pereteanu K, Luthi T, Niemz P (2007b) Determination of Young's and shear moduli of common yew and Norway spruce by means of ultrasonic waves. Wood Sci Technol 41:309–327

Keunecke D, Stanzl-Tschegg S, Niemz P (2007c) Fracture characterization of yew (*Taxus baccata* L.) and spruce (*Picea abies* [L.] Karst.) in the radial–tangential and tangential–radial crack propagation system by a micro wedge splitting test. Holzforschung 61:582–588

Krabbe E (1960) Messungen von Gleit- und Dehnungszahlen an Holzstäbchen mit rechteckigen Querschnitten. Dissertation, Hannover, p 106

Neuhaus FH (1981) Elastizitätszahlen von Fichtenholz in Abhängigkeit von der Holzfeuchtigkeit. Dissertation, Bochum, p 162

Reiterer A, Lichtenegger H, Tschegg S, Fratzl P (1999) Experimental evidence for a mechanical function of the cellulose microfibril angle in wood cell walls. Philos Mag A Phys Condens Matter Struct Defects Mech Properties 79(9):2173–2184

Schlüter R (1932) Elastische Messungen an Fichtenholz. Dissertation, Braunschweig, p 56

Sekhar AC, Sharma RS (1959) A note on mechanical properties of *Taxus baccata*. Indian Forest 85:324–326

Voigt W (1928) Lehrbuch der Kristallphysik. B.G. Teubner, Leipzig, p 960

Wagenführ R (2000) Holzatlas. Fachbuchverlag Leipzig, München, p 707

Wommelsdorff O (1966) Dehnungs- und Querdehnungszahlen von Hölzern. Dissertation, Hannover, p 100